Energy Systems Planning and Optimization

Journal home page: https://espo.kut.ac.ir

Research paper

Local Thermal Non-Equilibrium Analysis of Flow-Rate-Dependent Melting in an Encapsulated Paraffin Packed-Bed Storage System

Hooman Hadidi*

Department of Mechanical Engineering, Kermanshah University of Technology, Kermanshah, 67156-85420, Iran

Article Info

Received
24 July 2026

Revised
9 August 2026

Accepted
26 August 2026

Published online
5 September 2026

Keywords

Packed-bed;
Thermal energy storage;
PCM;
Paraffin;
LTNE;
Porous medium;

Abstract

This study presents a numerical investigation of the charging behavior of a vertical packed-bed latent heat thermal energy storage unit filled with spherical paraffin capsules. The capsule bed is modeled as a porous medium, and a local thermal non-equilibrium formulation is adopted to solve separate temperature fields for the water and PCM phases. The model includes porous flow resistance, interphase heat transfer, apparent heat capacity based on phase change, and heat loss from the insulated wall. The results indicate that the PCM temperature increases from about 54–55°C at 200 min to the melting range near 60°C at approximately 250 min. A clear latent-heat plateau is observed from about 250 to 490 min, after which the PCM temperature rises sharply, reaching approximately 66–68 °C. The water temperature remains higher than the PCM temperature during melting and exceeds 64 °C, confirming local thermal non-equilibrium. Phase-field contours show progressive melting from 300 to 900 min, with near-complete melting at 900 min. Flow-rate cases of 1.5, 2.5, 3.5, and 4.5 L/min demonstrate that the charging response depends strongly on the balance between convective transport and fluid residence time. The manuscript explicitly evaluates HTF temperature, PCM temperature, liquid fraction, pressure loss, and charging time as key model outputs.

* Corresponding author's Email address: h.hadidi@kut.ac.ir

 https://doi.org/ 10.22034/espo.2026.2095522.1007

1. Introduction

Solar energy, waste heat, and many other thermal energy inputs are inherently variable, resulting in a mismatch between energy availability and demand. Thermal energy storage (TES) is therefore required to improve system stability and energy utilization [1-6]. The simplest TES method is sensible heat storage (SHS), where heat is stored by increasing the temperature of a storage medium, such as water. Owing to its relatively high specific heat capacity, water is widely used for SHS; for instance, a 60 °C temperature rise in water corresponds to an energy storage capacity of about 250 MJ/m³. Nevertheless, sensible storage typically requires either a large storage capacity or a wide operational temperature spectrum.

Latent heat storage (LHS) operates differently employing phase-change materials (PCMs) to take in heat as they melt and release it again as they solidify. Because a considerable amount of energy can be stored as latent heat over a narrow temperature interval, PCM-based systems provide a higher volumetric energy density than conventional SHS systems [7-9]. Several reviews have reported that latent heat thermal energy storage (LHTES) units using PCMs may offer storage densities approximately 5–14 times greater than analogous sensible heat systems. As an example, paraffin-based storage can reduce the required storage volume by nearly 1.5 times in comparison to a water tank designed for the same energy capacity [10]. A useful feature of PCMs is that they stay near their melting or freezing temperature while storing or releasing heat. This renders the process almost isothermal, aids stabilizing temperature fluctuations, and can enhance better system efficiency. For these reasons, LHS has attracted considerable attention for solar thermal systems, buildings, and industrial waste-heat recovery applications.

The relative advantages of different TES technologies have been extensively examined in previous studies. Jouhara et al. [11] demonstrated that PCMs can store latent heat with minimal temperature variations , which makes them useful when heat supply and demand are not synchronous. Sharma et al. [12] made a similar point, explaining that LHS depends mainly on the enthalpy of phase change and therefore operates close to an isothermal condition. They also noted that common PCMs, including paraffin with a latent heat of about 200 kJ/kg, can store more energy during melting than many materials store through ordinary temperature rise, improving the storage density.

In some reported cases, organic PCM-based LHS systems have achieved energy densities up to one order of magnitude greater than comparable sensible heat storage systems. In addition, Jouhara et al. [11] emphasized that encapsulation methods, including shape stabilization as well as micro- and macro-encapsulation, are important for the practical implementation of PCM-based thermal storage systems.

Encapsulated PCM packed-bed tanks represent a prevalent configuration for latent heat storage systems [2, 13-16]. In this configuration, PCM-filled capsules, commonly spherical but sometimes of other geometries, are placed randomly inside a storage vessel. A heat-transfer fluid (HTF), such as water or air, circulates across the void spaces between the capsules during charging and discharging processes. During charging, the HTF transfers heat to the PCM, facilitating its melting, whereas during discharging the stored heat is released as the PCM solidifies [16-20]. Compared with other LHTES configurations, such as shell-and-tube units, packed beds can provide a large heat-transfer surface area and a high packing density. The spaces between the capsules also allow the HTF to remain in direct thermal contact with the encapsulated PCM.

The modeling of packed-bed thermal systems originates from early studies on gas–solid two-phase heat transfer. Later studies, such as those by Saitoh and Hirose [21] and Beasley et al. [22], adapted the initial models to encompass phase transition phenomena. . Regin et al. [23] reported that packed-bed LHTES systems have been applied in solar heating, thermal storage for air-conditioning, building heating, and waste-heat recovery. They emphasized that the significant surface-to-volume ratio and improved storage capacity of packed beds renders them appealing compared with bulk PCM storage systems. More recent reviews, such as those by Grabo et al. [24] and de Gracia and Cabeza [25], also indicate that spherical PCM capsules remain the most commonly investigated geometry. In general, numerical models for packed-bed LHTES can be grouped into four categories: homogeneous single-phase models, Schumann-type two-phase models, concentric-dispersion or cell-based models, and fully resolved two-phase finite-element models.

The performance of a packed-bed LHTES unit is strongly influenced by several design and operating parameters, including capsule diameter, porosity, tank geometry, HTF flow rate, and PCM thermophysical properties [26-29]. Earlier studies [30-35] found that smaller capsules usually conduct heat rapidly due to their increased surface area relative to their volume. For instance, Mao and Cao [29] demonstrated numerically that smaller capsule diameters enhance the overall storage behavior. Porosity also plays an important role: a more permeable bed lowers the pressure drop but may decrease the available heat-transfer area. In contrast, highly compact arrangements, such as face-centered packing with porosity near 32%, can intensify heat exchange. Moreover, when the capsule diameter is not small compared with the tank dimensions, considerable spatial temperature variations may develop. This issue advocates for the use of local thermal nonequilibrium models rather than assuming a single temperature for the HTF and PCM phases.

Packed-bed LHTES units may operate either as purely latent storage systems or as hybrid sensible–latent storage devices. In some cases, the HTF itself contributes to sensible heat storage while simultaneously transferring heat to the PCM capsules. For example, in the experimental study of Nallusamy et al. [36], water inside a 250 L tank provided sensible storage while paraffin-filled capsules acted as the latent storage medium. This study examined how inlet temperature, flow rate, and bed porosity affect charging by tracking heat stored at each moment, total stored energy, charging rate, and thermal efficiency. Experimental studies of this type underline the main performance indicators of packed-bed LHTES systems, including complete melting time, stored energy per unit mass or volume, and thermodynamic efficiency. Reported charging durations vary widely, from several hours for moderate-size systems and relatively high heat input to much longer periods for large beds or low-flow operating conditions. In most cases, efficiency is estimated by comparing the useful latent heat taken up by the PCM with the ideal storage capacity, after allowing for heat losses.

Paraffin wax is widely used as a PCM in low-temperature latent heat storage due to its practicality and compatibility with this temperature range. In packed-bed configurations, the paraffin is enclosed within capsules to retain the molten PCM and simplify system handling. These capsules are commonly constructed from polymeric or metallic materials and typically have diameters in the range of about 0.03–0.1 m. Encapsulation isolates the PCM from the heat-transfer fluid (HTF), prevents leakage during melting, and enables the use of geometries that can enhance heat-transfer area, such as spherical, finned, or other modified capsule shapes. Nevertheless, conventional spherical capsules provide a relatively limited surface-area-to-volume ratio. As discussed by Grabo et al., decreasing the capsule diameter is one of the simplest methods for increasing this ratio and optimizing heat exchange. Although fins and non-spherical capsules have been investigated experimentally, uncomplicated spherical capsules remain the dominant choice in large-scale storage tanks because of their easier fabrication and practical applicability.

Although phase change materials, encapsulated latent heat storage, and packed-bed thermal storage systems have been extensively studied, further numerical work is still needed to link PCM selection and operating conditions within a unified and physically realistic model. Many existing investigations focus individually on material properties, capsule design, heat-transfer enhancement techniques, or flow parameters. However, fewer studies clearly examine the combined influence of a practical operating variable, such as inlet flow rate, and a material-related parameter, such as PCM melting temperature, on the charging behavior of a packed-bed LHS system.

This issue is significant because the performance of encapsulated PCM beds depends not only on the latent heat capacity of the selected material, but also on the rate at which thermal energy is transported by the HTF and transferred to the PCM inside the capsules. Increasing the flow rate can promote faster heat delivery, shorten the melting period, and improve the charging response, but it may also lead to a higher pressure drop and greater pumping power demand. In the same way, using a PCM with a lower melting point may allow latent heat absorption to begin earlier, whereas a PCM with a higher melting point can store heat at a more useful elevated temperature but may require a longer time to melt completely.

Therefore, the present work is driven by the need to investigate these interacting effects through a validated numerical model of a packed-bed latent heat storage unit. By considering a reference case and comparing it with selected changes in inlet flow rate and PCM melting temperature, this study seeks to clarify the key thermal and hydraulic compromises that govern charging performance. The main evaluated parameters include temperature development, liquid-fraction progression, complete charging time, and pressure loss. This modeling strategy offers a concise yet informative basis for improving the design and operation of packed-bed latent heat storage systems used in solar thermal and low-temperature energy-storage applications.

2. Model Description and Theoretical Formulation

2.1. Problem definition

This study examines the time-dependent charging performance of a packed-bed latent heat thermal energy storage system. The storage device is composed of a vertical cylindrical vessel packed with spherical capsules that contain a phase change material (PCM). Water served as the heat-transfer fluid (HTF). During charging, hot water flows in from the bottom, ascends through the capsule bed, transfers thermal energy to the encapsulated PCM, and subsequently departs out through the outlet at the top. The supplied heat is initially accumulated in the PCM as sensible energy and then as latent heat during the melting process.

The problem involves the simultaneous interaction of fluid motion, heat transport, and phase transformation. The flow of the HTF through the capsule assembly is represented as porous-medium flow, while the PCM-filled capsules are considered the solid matrix of the porous structure. Since the capsule diameter is not negligible relative to the tank dimensions, local thermal equilibrium between the water and PCM cannot be assumed. Accordingly, a local thermal nonequilibrium formulation is used, in which the fluid phase and the PCM/solid matrix phase are characterized by separate temperature fields.

The numerical model is developed to determine the transient variation of the HTF temperature, PCM temperature, melt fraction, pressure loss, and the time required to complete the charging process. In the reference case, the storage tank is initially at a uniform temperature of 29°C. Water flows upward through the packed bed at a baseline flow rate of 1, 2, 3, and 4 L/min, while the solar heating circuit provides 400 W of thermal input. Paraffin is selected as the reference PCM, with a melting point of 62°C and a latent heat of fusion of 230 kJ/kg.

2.2. Geometry and computational domain

Figure 1 presents the physical configuration of the packed-bed latent heat thermal storage system considered in this study. The storage unit is arranged as a vertical cylindrical vessel in which the heat-transfer fluid enters from the lower section and leaves from the upper section. The active storage zone is located inside the tank and is occupied by randomly packed spherical capsules containing the phase change material. Around the storage region, a glass-wool insulation layer is included to restrict thermal interaction with the ambient environment. During the charging process, hot water is supplied through the bottom inlet, flows upward through the void spaces between the encapsulated PCM particles, transfers heat to the PCM capsules, and finally exits through the outlet at the top of the tank.

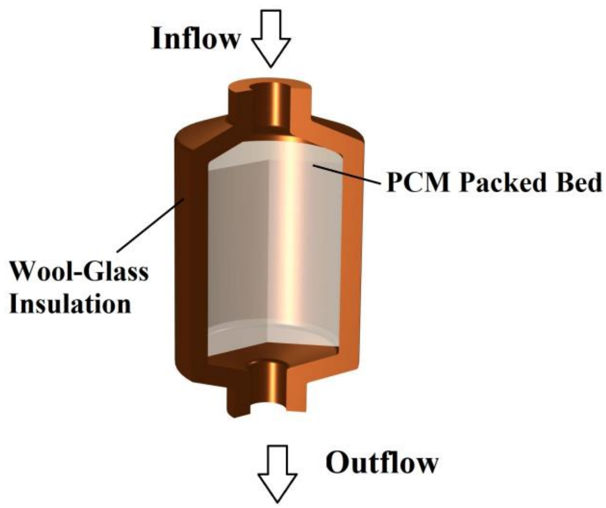

Fig. 1. Physical layout of the vertical packed-bed latent heat storage tank, including the lower inlet, upper outlet, PCM capsule bed, and external glass-wool insulation.

Owing to the rotational symmetry of the cylindrical tank, the full three-dimensional geometry is represented by a two-dimensional axisymmetric computational domain. This simplification considerably decreases the numerical expense while maintaining the essential radial and axial variations of temperature and flow inside the storage unit. The tank diameter and height are 0.40 m and 0.50 m, respectively. The PCM capsules have a diameter of $d_p = 60$ mm, and the porosity of the packed region is $\varepsilon_p = 0.52$.

The numerical domain is separated into four physical subregions. The lower section corresponds to the inlet zone, where the HTF is introduced into the system. The middle part represents the packed-bed storage region, which is modeled as a porous zone filled with spherical PCM capsules. The upper section is assigned as the outlet zone, where the fluid leaves the tank after exchanging heat with the PCM. The outer layer represents the glass-wool insulation surrounding the tank wall.

In the present model, the geometry of each capsule is not individually resolved. Instead, the packed capsule assembly is replaced by an equivalent homogeneous porous medium. This representation is appropriate for the present objective because the study focuses on the macroscopic charging response of the entire storage tank, including temperature evolution, melting progress, and pressure loss, rather than the microscopic thermal gradients inside individual capsules.

2.3. Modeling assumptions

The mathematical model is formulated based on the following assumptions. The storage tank is considered axisymmetric, while the packed capsule bed is approximated as a uniform porous medium. The flow field is calculated as a steady-state field during charging, while the thermal problem is solved in a transient manner. Since the temperature of the flowing water and that of the encapsulated PCM may differ locally, a local thermal nonequilibrium formulation is employed. In this approach, separate temperature fields are assigned to the HTF and the PCM/solid matrix. Natural convection within the PCM capsules is overlooked ; therefore, the PCM is treated as a solid or immobile liquid during phase change. Heat exchange with the surroundings transpires exclusively through convective heat loss from the outer insulated wall.

The use of a stationary flow field is supported by the relatively low flow velocity in the packed region. In the reference condition, the maximum velocity is approximately 6 mm/s, corresponding to a Reynolds number close to 600. At this condition, the velocity distribution is assumed to be weakly influenced by the transient temperature field. Therefore, solving the flow field independently before the transient thermal calculation provides a reasonable reduction in computational effort while preserving the dominant physics of the charging process.

2.4. Governing equations

2.4.1. Solar-loop energy balance

The inlet temperature of the water was calculated from the thermal power supplied by the solar collector. The energy balance between the inlet and outlet of the tank can be written as

$$\dot{Q}_u = \dot{V}_{in}\rho_f C_{p,f}(T_{in} - T_{out}) \tag{1}$$

where $\dot{Q}_u$ is the useful heat supplied by the solar collector, $\dot{V}_{in}$ is the volumetric flow rate of water, ρ_f is the density of water, $C_{p,f}$ is the specific heat capacity of water, and T_{in} and T_{out} are the inlet and outlet temperatures of the HTF, respectively.

Accordingly, the inlet temperature imposed at the lower boundary of the tank is obtained as

$$T_{in} = T_{out} + \frac{\dot{Q}_u}{\dot{V}_{in}\rho_f C_{p,f}} \tag{2}$$

In the reference case, the heating power is $\dot{Q}_u = 400$ W. The initial temperature of the storage unit is assumed to be uniform.

2.4.2. Flow formulation in the packed bed

The water flow through the PCM capsule bed was described using a porous-medium approach. Since the capsule bed introduces both viscous and inertial resistance, the pressure drop was calculated using the Ergun relation. The momentum resistance in the packed region is expressed as

$$\nabla p = -\frac{\mu_f}{\kappa}\mathbf{u} - \frac{1.75(1-\varepsilon_p)}{d_p\varepsilon_p^3}\rho_f \mid \mathbf{u} \mid \mathbf{u} \tag{3}$$

where p is pressure, μ_f is the dynamic viscosity of water, κ is the permeability of the packed bed, $\mathbf{u}$ is the superficial velocity vector, and $d_p$is the capsule diameter.

The permeability of the packed bed is evaluated by

$$\kappa = \frac{d_p^2 \varepsilon_p^3}{150(1-\varepsilon_p)^2} \tag{4}$$

The Reynolds number in the packed region is estimated as

$$Re_p = \frac{d_p v \rho_f}{(1-\varepsilon_p)\mu_f} \tag{5}$$

where v is the characteristic velocity in the bed. In the benchmark condition, the maximum velocity is approximately 6 mm/s, which gives a Reynolds number of about 600. Therefore, the velocity field was considered independent of the transient temperature field, and a stationary flow solution was first obtained. This stationary flow field was then used in the transient heat-transfer calculation.

2.4.3. Local thermal nonequilibrium treatment

Because the PCM capsules are relatively large compared with the tank dimensions, the water and PCM temperatures may differ locally during charging. Therefore, a local thermal nonequilibrium approach was adopted. In this method, the water temperature and the PCM matrix temperature are solved separately.

The thermal interaction between the water and the encapsulated PCM is represented by an interphase heat source. The heat transferred from the PCM capsule phase to the water phase is written as

$$Q_f = \frac{q_{sf}}{\varepsilon_p}\left(T_s - T_f\right) \tag{6}$$

where Q_f is the heat source term in the fluid phase, T_s is the PCM or solid-matrix temperature, T_f is the HTF temperature, and q_{sf} is the volumetric interstitial heat-transfer coefficient.

For spherical capsules, q_{sf} is defined as

$$q_{sf} = \frac{6(1-\varepsilon_p)}{d_p} h_{sf} \tag{7}$$

where h_{sf} is the interfacial heat-transfer coefficient between the water and the capsule surface.

The interfacial heat-transfer coefficient is obtained from the Nusselt number as

$$h_{sf} = \frac{Nu\, k_f}{d_p} \tag{8}$$

where Nu is the Nusselt number and k_f is the thermal conductivity of water.

The Prandtl number of the HTF is calculated by

$$Pr = \frac{\mu_f C_{p,f}}{k_f} \tag{9}$$

In the present model, natural convection inside the PCM capsules is neglected. Therefore, the PCM is treated as a solid or immobile liquid during the phase-change process.

2.4.5. Phase-change modeling

The melting of paraffin was included using an apparent heat-capacity formulation. The PCM stores energy as sensible heat before reaching the melting range and then absorbs latent heat during the solid–liquid transition. The liquid fraction, λ, varies from 0 for the solid state to 1 for the fully melted state:

$$\lambda = \begin{cases} 0, & T_s < T_m - \dfrac{\Delta T_m}{2} \\ \dfrac{T_s - \left(T_m - \frac{\Delta T_m}{2}\right)}{\Delta T_m}, & T_m - \dfrac{\Delta T_m}{2} \le T_s \le T_m + \dfrac{\Delta T_m}{2} \\ 1, & T_s > T_m + \dfrac{\Delta T_m}{2} \end{cases} \tag{10}$$

where T_m is the melting temperature and ΔT_m is the melting interval.

The effective heat capacity of the PCM is then written as

$$C_{p,pcm}^{eff} = C_{p,pcm} + L\frac{d\lambda}{dT_s} \tag{11}$$

where L is the latent heat of fusion.

For the melting interval,

$$\frac{d\lambda}{dT_s} = \frac{1}{\Delta T_m} \tag{12}$$

and therefore,

$$C_{p,pcm}^{eff} = C_{p,pcm} + \frac{L}{\Delta T_m} \tag{13}$$

This approach allows the latent heat effect to be included as an additional heat-storage capacity over the selected phase-change temperature range.

2.4.6. Boundary conditions

At the start of the simulation, the entire tank is initialized at a uniform temperature:

$$T_f(r, z, 0) = T_s(r, z, 0) = T_0 \tag{14}$$

At the inlet, a fully developed flow condition is prescribed, and the inlet temperature is calculated from Eq. (2). At the outlet, a pressure boundary condition is applied. The solid walls are treated with a no-slip condition for the fluid flow.

The heat loss from the external surface of the insulation is modeled using a convective heat-flux boundary condition:

$$-k_{ins}\frac{\partial T}{\partial n} = h_{amb}(T_{wall} - T_{amb}) \quad (15)$$

where k_{ins} is the thermal conductivity of the insulation, h_{amb} is the external convective heat-transfer coefficient, $T_{wall}$is the outer wall temperature, and T_{amb} is the ambient temperature. In this study, $h_{amb} = 5$ W/(m^{2}K).

2.5. Numerical solution procedure

The simulation was performed in two sequential steps. First, the flow field was solved under steady-state conditions. Then, the resulting velocity distribution was used in the transient thermal simulation, which solved the heat-transfer problem accounting for phase change and local thermal nonequilibrium between the HTF and PCM phases.

The main outputs of the model are the HTF temperature, PCM temperature, liquid fraction, pressure drop, and total charging time. The charging process is considered complete when the PCM temperature reaches the selected final charging temperature throughout the storage region.

2. 6. Grid Independence Study

Several mesh sizes were tested to ensure that the numerical results did not depend on how finely the domain was divided. For this purpose, four meshes with approximately 3,000, 6,000, 13,000, and 19,000 nodes were generated and simulated using the same physical properties, operating conditions, and boundary conditions.

The predicted PCM temperature histories obtained from these meshes are compared in Figure 2. The curves corresponding to the 3,000-node and 6,000-node meshes show noticeable differences from those obtained with the finer grids, indicating that these relatively coarse meshes do not provide sufficient spatial resolution to accurately capture the transient heat-transfer and phase-change behavior inside the packed-bed storage unit.

When the mesh density was increased to 13,000 nodes, the PCM temperature response became very close to that predicted using the 19,000-node mesh. The difference between these two refined cases is minimal, indicating that further mesh refinement has no significant influence on the calculated temperature evolution. Therefore, the mesh with 13,000 nodes was adopted for the remaining simulations, as it provides an appropriate compromise between numerical accuracy and computational cost.

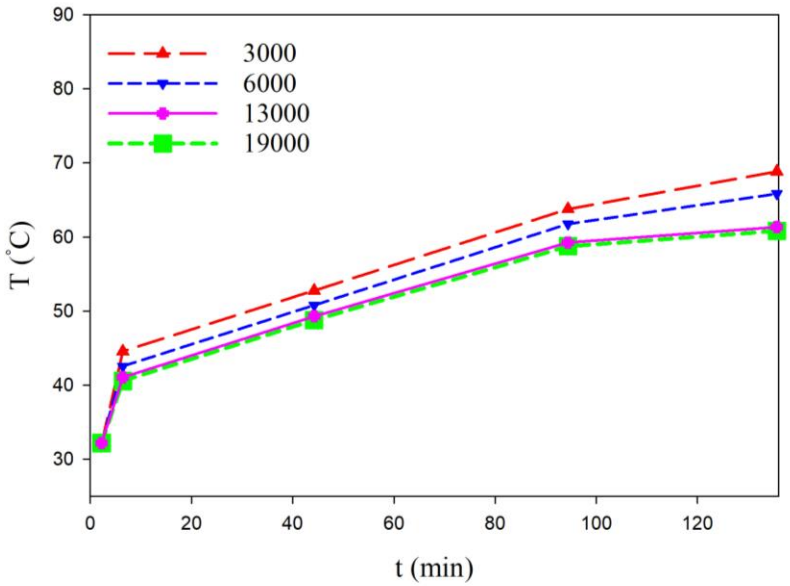

Fig. 2. Mesh independence assessment based on the transient PCM temperature response during charging for different grid resolutions

3. Results and Discussion

3.1. Model Validation

The numerical model was validated by comparing its predicted charging response with the experimental measurements of Nallusamy et al. (2006) for a packed-bed latent heat thermal energy storage unit.

Figure 3 presents the transient PCM temperature during the charging period. The experimental measurements, shown by black triangular markers, are compared with the numerical results obtained in the present study, represented by the red dashed curve.

The comparison indicates that the simulated temperature profile follows the experimental trend with good consistency throughout the charging process. In both cases, the PCM temperature evolution shows the main thermal stages of latent heat storage: an initial sensible heating period, a phase-change interval in which the temperature rise slows due to latent heat absorption, and a final sensible heating stage after most of the PCM has melted.

The small differences between the measured and computed results may be related to several unavoidable modeling simplifications, including possible variations in heat loss through the tank insulation, nonuniform flow distribution within the real packed bed, uncertainties in experimental measurements, and the use of idealized thermophysical properties in the numerical model.

Despite these minor deviations, the numerical model reproduces the transient heating and melting behavior of the packed-bed PCM system with satisfactory accuracy. Therefore, the model can be considered reliable for investigating the influence of operating and material parameters on the charging performance of the TES unit.

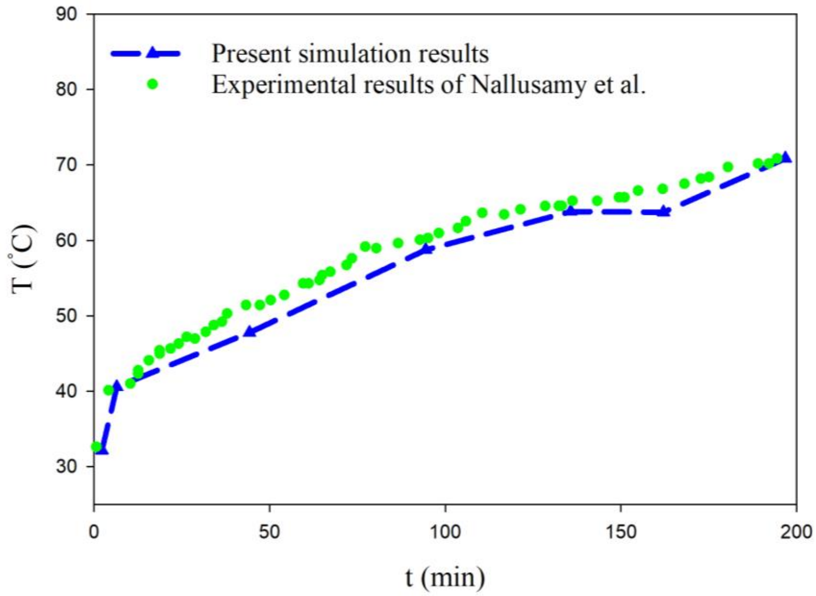

Fig. 3. Validation of the numerical model through comparison of the simulated PCM temperature profile with the experimental data of Nallusamy et al. [36] during charging.

3.2. Transient thermal response of the fluid, PCM, and averaged porous medium

Figure 4 presents the temporal variation of the PCM temperature, water temperature, and volume-averaged porous-medium temperature during the charging process. The selected time interval covers the most important part of the thermal response, including the approach to the melting temperature, the phase-change period, and the transition toward post-melting sensible heating. The three curves exhibit different thermal behaviors, reflecting the local thermal nonequilibrium between the flowing heat-transfer fluid and the encapsulated PCM.

At the beginning of the plotted interval, around $t = 200$ min, the three temperatures are close to 54–55°C. From 200 to approximately 250 min, all curves increase rapidly and approach the melting temperature of the PCM, which is around 60°C. At this stage, the PCM is still mainly in the solid state, and the supplied heat is stored predominantly as sensible energy. The water temperature is slightly higher than the PCM temperature because the water acts as the heat-transfer carrier to the PCM capsules.

After approximately 250 min, the PCM temperature reaches the melting region and its slope decreases significantly. Between about 250 and 490 min, the PCM temperature remains almost constant near 60°C. This plateau is the main indication of latent heat storage: during this period, the heat transferred from the water is not primarily used to increase the PCM temperature but is instead consumed in the solid–liquid phase transition. Therefore, the PCM temperature changes only slightly while melting progresses within the storage bed.

The water temperature behaves differently from the PCM temperature during this interval. Unlike the PCM curve, the water temperature continues to increase gradually from approximately 60°C to above 64°C. This difference shows that the heat-transfer fluid and the PCM are not in thermal equilibrium during charging: the flowing water responds directly to the inlet heating condition and convective transport, whereas the PCM temperature is constrained by latent heat absorption. This separation between the water and PCM temperatures confirms that a local thermal nonequilibrium formulation is necessary for the present packed-bed model.

The volume-averaged porous-medium temperature follows an intermediate trend between the PCM and water curves. During the phase-change period, it remains close to the PCM temperature but is slightly higher because it includes the contribution of the hotter fluid phase. This averaged temperature is useful for describing the overall local thermal state of the storage medium, but it does not fully represent either the fluid or PCM response individually. Therefore, plotting the three temperatures together provides a clearer interpretation of the coupled heat-transfer process.

A sharp increase in the PCM temperature occurs after approximately 495–500 min. This sudden rise indicates that the local melting process is nearly completed and that the PCM begins to store additional heat mainly as sensible heat in the liquid phase. At nearly the same time, the volume-averaged porous-medium temperature also increases rapidly, confirming the transition from latent-dominated storage to post-melting sensible heating. The water temperature, however, changes more smoothly because it is continuously transported through the bed and is less restricted by the phase-change temperature.

Toward the end of the plotted period, all three curves converge and reach approximately 66–68°C. The reduction in the temperature difference among the phases indicates that the thermal nonequilibrium weakens after the main melting stage. Once most of the PCM has changed phase, the latent heat buffering effect decreases and the PCM temperature can rise more freely. As a result, the PCM, water, and averaged porous-medium temperatures gradually approach a more uniform thermal condition.

Overall, Figure 4 shows that charging occurs in three main stages. First, the system heats sensibly before the PCM begins to melt, so all temperatures increase quickly. Next, the PCM absorbs latent heat and remains close to its melting temperature, while the water continues to warm. Finally, after most of the PCM has melted, its temperature rises more quickly and the water and PCM temperatures converge. These results clearly show the importance of separating the fluid and PCM temperatures in the numerical model, since a single-temperature formulation would not capture the thermal delay caused by phase change.

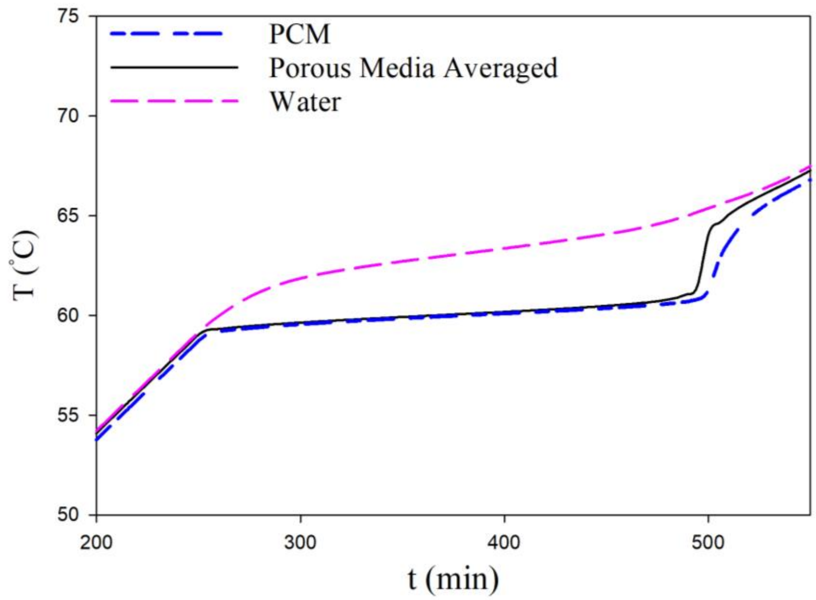

Fig. 4. Time evolution of PCM temperature, water temperature, and volume-averaged porous-medium temperature during the charging process.

3.3. Effect of Inlet Flow Rate on PCM Temperature Evolution

Figure 5 shows that the inlet flow rate has a clear effect on the evolution of the PCM temperature during charging. The simulations considered four flow rates: 1.5, 2.5, 3.5, and 4.5 L/min. As results show, the heating and melting rate is strongly dependent on the amount of HTF passing through the bed.

It is obvious that the flow rate has an effect on the time of heating and melting of the PCM. At 1.5 L/min, the PCM is heating for longer time and melting happens later. The main reason is that less water is flowing through the bed, thus the heat transfer from water to capsules is weaker. For this reason, the temperature stays near the melting range for a longer time.

Higher flow rates (2.5 and 3.5 L/min) cause the PCM to begin melting earlier and this is due to the fact that the moving heat-transfer fluid (water) transports heat more efficiently through the packed bed. Consequently, the PCM temperature increases more quickly and the melting time decreases. These results demonstrate that an increased flow rate can improve the charging process by enabling the heat to spread more quickly throughout the bed.

The fastest heating takes place at 4.5 L/min. At this flow rate, the water flows sooner and transfers heat to the capsules in less time, which causes the PCM to reach its melting point faster. However, high flow rates may also cause some uneven heating, especially near the inlet where the hot water first enters the storage unit. This suggests that faster charging does not always guarantee the best temperature distribution.

In general, the flow rate must be chosen carefully. A lower flow rate leads to a slower charging process while a very high flow rate may result in less uniform heating. From the comparison, the intermediate flow rates, especially around 2.5–3.5 L/min, appear to provide a more balanced performance heating the PCM at a reasonable speed while minimizing temperature variation within the bed.

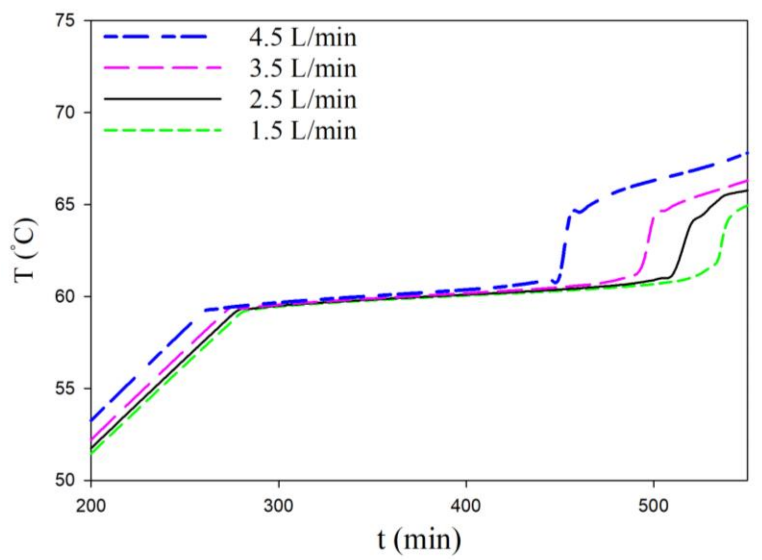

Fig. 5. Domain-averaged PCM temperature during charging for inlet flow rates of 1.5, 2.5, 3.5, and 4.5 L/min. The curves show how the flow rate changes the start and development of PCM melting.

3.4. Transient temperature and streamline development during charging

Figure 6 presents the coupled temperature field and streamline distribution inside the packed-bed latent heat storage unit at four charging times: 15, 270, 420, and 900 min. These times represent the early stage of charging, the intermediate heating period, the later transient stage, and the final long-time thermal condition. The temperature contours show the spatial development of the thermal field, while the streamlines illustrate the path of the heat-transfer fluid through the storage domain.

At 15 min, shown in Figure 6(a), the temperature field remains close to the initial state, varying only slightly, , approximately between 21.8°Cand 25.1°C. This indicates that the charging process has just begun and that only a limited amount of heat has been transferred to the storage medium. The streamlines show that the fluid enters through the lower inlet, spreads into the packed-bed region, and then moves toward the outlet. The flow pattern is already fully established at this early time, but the thermal response of the packed bed remains weak because the PCM and surrounding porous region have not yet absorbed a significant amount of energy.

At 270 min, shown in Figure 6(b), the temperature distribution becomes more developed. The maximum temperature is approximately 24.8°C, while the minimum temperature near the outer boundary is about 20.3°C. A clearer thermal gradient appears near the outer wall and insulation side. This indicates that heat is no longer confined mainly to the central flow path. Both conduction and convection are now affecting a wider part of the tank. The streamline pattern still looks much like it did earlier, indicating a nearly steady flow field , even though the temperature field continues to evolve . The closer streamlines near the inlet and outlet show stronger local fluid motion, which can enhance heat transfer in those areas.

At 420 min, shown in Figure 6(c), the temperature field continues to change, with the maximum temperature decreasing slightly to about 24.4°Cand the minimum value remaining close to 20.2°C. The thermal contours show a more extended temperature gradient along the wall and outlet-side regions. This suggests that heat redistribution within the storage domain has become more pronounced. The streamlines still follow the same main flow route, moving upward through the packed bed and bending near the outlet. This nearly unchanged streamline structure confirms that the transient behavior observed in the figure is mainly thermal rather than hydrodynamic.

At the long charging time of 900 min, Figure 6(d), the temperature field reaches a more developed condition, but noticeable spatial nonuniformity remains. The maximum temperature is approximately 22.8°C, while the minimum temperature is about 20.1°C. Compared with the earlier panels, the high-temperature region becomes less intense, and the contours indicate a smoother temperature distribution. This suggests that the system is approaching a more stable thermal state. However, the persistence of temperature gradients near the outer boundary shows that radial thermal resistance and wall heat exchange still influence the local temperature field even after a long operating time.

The streamline pattern in all four panels is generally similar, showing that the fluid-flow structure is established rapidly and remains almost unchanged throughout the thermal transient. The main flow passes through the packed region and bends near the inlet and outlet transitions. This is significant because it identifies where convection contributes the most to heat transfer. Regions crossed by denser streamlines experience stronger fluid–solid interaction, while areas away from the main flow path are more affected by conduction and wall heat transfer. Therefore, the temperature field is shaped not only by the imposed thermal boundary conditions but also by the flow distribution within the packed bed.

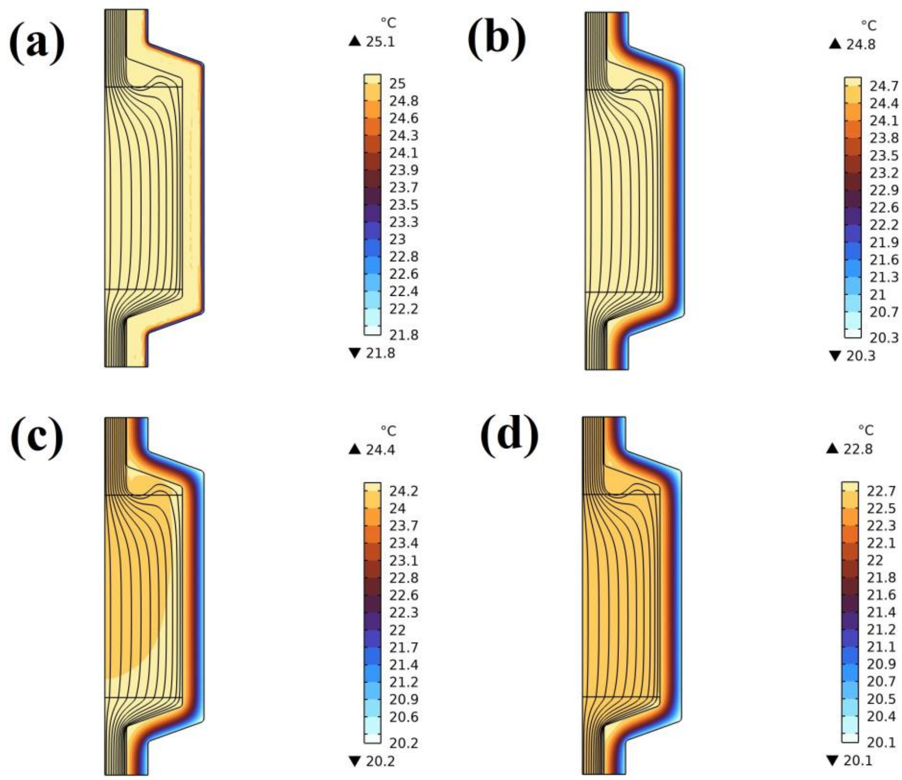

Fig. 6: Temperature contours and streamline distribution in the packed-bed latent heat storage unit at different charging times: (a) 15 min, (b) 270 min, (c) 420 min, and (d) 900 min.

3.5. Effect of inlet flow rate on PCM temperature distribution

Figure 7 presents the PCM temperature contours at $t = 480$ minfor four inlet flow rates of 1, 2, 3, and 4 L/min. This time corresponds to the phase-change-dominated period of the charging process, in which the PCM temperature is close to the melting range and the effect of flow rate on the thermal field can be clearly observed. In all cases, the PCM temperature remains mainly within a narrow range around 60°C, confirming that latent heat absorption still controls the thermal response of the packed bed at this time.

For the lowest inlet flow rate, $\dot{V}_{in} = 1$ L/min, shown in Figure 7(a), the PCM temperature varies approximately from 59.5°Cto 65.5°C. A relatively large high-temperature region is observed inside the packed bed, particularly near the upper and central parts of the domain. This indicates that a noticeable portion of the PCM has already passed through the melting range and entered the sensible-heating stage of the liquid PCM. The higher temperature level in this case can be attributed to the longer residence time of the heat-transfer fluid in the bed and the larger temperature rise of the fluid under the fixed heat-input condition.

When the inlet flow rate increases to $\dot{V}_{in} = 2$ L/min, Figure 7(b), the temperature field becomes more concentrated near the melting range. The contour values are approximately between 59.7°Cand 60.7°C. Compared with the 1 L/mincase, the temperature rise above the melting point is significantly smaller. This shows that the PCM is still mainly undergoing phase change and that the post-melting sensible-heating region is less developed. Although the flow rate is higher, the water temperature rise per circulation is lower, reducing the effective temperature difference available for heating the PCM.

At $\dot{V}_{in} = 3$ L/min, shown in Figure 7(c), the PCM temperature remains approximately within 59.7°C–60.5°C. The thermal field is still strongly constrained by the phase-change process. Most of the packed bed remains close to the melting temperature, indicating that the latent heat storage stage is still dominant. The contour pattern shows that increasing the flow rate from 2to 3 L/mindoes not substantially raise the PCM temperature at the selected time. Instead, the PCM temperature field remains buffered by latent heat absorption.

For the highest flow rate, $\dot{V}_{in} = 4$ L/min, Figure 7(d), the PCM temperature is also close to the melting interval, with values approximately between 59.8°Cand 60.4°C. The temperature distribution is relatively narrow, which indicates that the PCM is still mainly in the phase-change stage. The limited temperature rise above 60°Csuggests that the higher flow rate does not lead to faster sensible heating of the PCM after melting. Instead, the shorter fluid residence time and lower temperature rise of the heat-transfer fluid delay the transition to the post-melting stage.

The comparison among Figures 7(a)–(d) shows that the 1 L/mincase produces the most advanced thermal state at 480 min, while the higher-flow-rate cases remain closer to the melting temperature. This behavior is important as it shows that increasing inlet flow rate does not necessarily improve the PCM temperature response when the supplied heating power is fixed. Under a constant heat input, increasing the flow rate reduces the temperature gain of the fluid, so the water entering and circulating through the storage region carries heat at a lower temperature level. In addition, the residence time of the fluid within the packed bed decreases, limiting the duration of heat exchange between the fluid and the PCM capsules.

The results therefore reveal a competition between convective transport and residence time. A higher flow rate increases fluid circulation and may enhance the convective heat-transfer coefficient, but this advantage can be offset by the lower fluid temperature rise and reduced contact time. By comparison, a lower flow rate gives the water more time inside the tank, enabling it to transfer more heat to the PCM, which can result in a higher local PCM temperature at the same charging time.

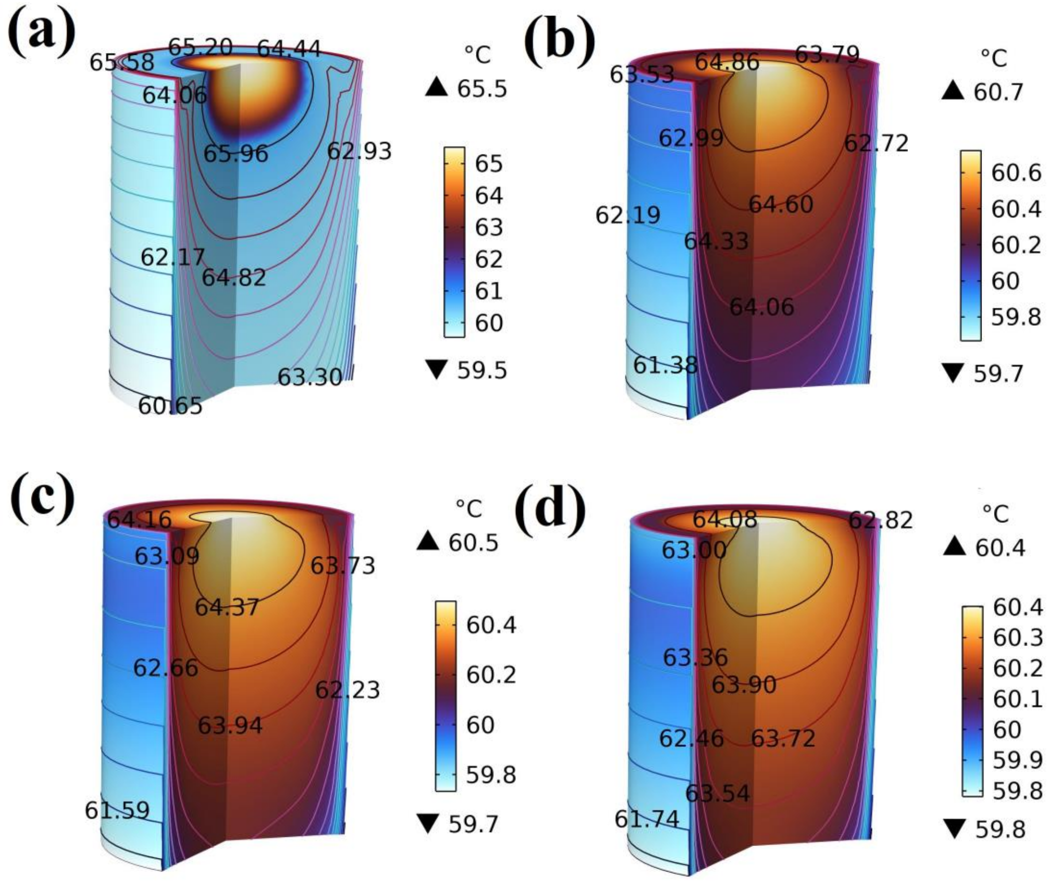

Fig. 7. PCM temperature contours at $t = 480$ minfor different inlet flow rates: (a) $\dot{V}_{in} = 1$ L/min, (b) $\dot{V}_{in} = 2$ L/min, (c) $\dot{V}_{in} = 3$ L/min, and (d) $\dot{V}_{in} = 4$ L/min.

3.6. Phase-field evolution during the PCM melting process

Figure 8 illustrates the evolution of the phase field within the storage unit during the charging process at four different times, namely 300, 420, 540, and 900 min. The phase-field variable varies between 0 and 1, representing the local progression of phase change within the PCM domain. As charging proceeds, the contours clearly show the gradual expansion of the melted region and the corresponding retreat of the solid phase. The figure therefore provides a direct visualization of how the melting front propagates spatially over time.

At 300 min (Fig. 8(a)), melting is already well established, but the PCM is still far from fully liquefied. Much of the domain still has medium or low phase-field values, which means a noticeable amount of PCM is still solid or only partially melted. The highest phase-field values are concentrated mainly in regions that receive thermal energy more effectively from the circulating fluid. In contrast, lower values persist in thermally less accessible regions, showing that melting is nonuniform at this stage. This behavior is expected as the charging process begins with strong local heating near the fluid pathways, while heat penetration toward the more remote regions remains limited.

At 420 min (Fig. 8(b)), the melted zone expands noticeably. Compared with the 300 min case, a larger fraction of the PCM reaches higher phase-field values, indicating significant advancement of the melting process. The low-value regions shrink and become confined to smaller zones, mainly where thermal resistance is greater and heat penetration is slower. This confirms that the latent heat absorption stage is actively progressing, with the melting front is moving from the initially heated regions toward the rest of the domain. The contours also suggest that the internal thermal field becomes more developed with time, leading to more effective heat diffusion and a smoother spatial distribution of the phase field.

By 540 min (Fig. 8(c)), the PCM is close to the final stages of melting. Most areas show high phase-field values, suggesting that much of the material has already melted or is nearly fully melted. Only limited regions with lower values remain, indicating that the solid phase persists mainly in the most thermally delayed parts of the storage volume. At this stage, the overall melting front becomes less sharp than at earlier times because a large part of the domain has already transitioned to the liquid state. This suggests that the charging process is moving from a strongly transient melting regime toward the final completion stage. At 900 min (Fig. 8(d)), the phase field becomes nearly uniform and close to its upper limit throughout the domain, showing that the PCM is almost completely melted. The absence of low phase-field values shows that the solid PCM has almost completely disappeared by the end of charging. Since the phase field is nearly uniform, the system is in a late charging stage: added heat now mostly raises the temperature of the melted PCM instead of driving further melting. This suggests that most of the latent heat storage capacity has already been utilized.

Overall, the phase-field contours show that melting develops gradually and is not uniform at first. During the early and middle stages, some regions melt faster because they exchange heat more effectively with the HTF. Over time, the melting front spreads across the domain, the liquid fraction increases, and the differences between regions diminish. This type of gradual smoothing is common in latent heat storage, where both fluid convection and heat conduction through the PCM control how melting progresses.

Figure 8 also makes clear that melting is not immediate, even after several hours of charging. The partly melted zones still visible at 300 and 420 min show that internal thermal resistance limits how quickly heat can move into the PCM. Even at 540 min, some regions still lag behind the rest of the domain. This indicates that the completion of melting depends not only on the supplied heat but also on the geometry of the storage unit, the fluid flow distribution, and the local heat-transfer pathways. Such behavior is important from a design viewpoint because it shows that improving flow uniformity and heat-transfer effectiveness can significantly shorten the total charging time.

In summary, Figure 8 confirms that the phase-field variable is a powerful indicator of the melting dynamics in the storage system. The contours reveal a clear transition from a partially melted state at 300 min, to an expanded melting front at 420 min, to near-complete melting at 540 min, and finally to an almost fully melted domain at 900 min. These results provide strong evidence that the charging process is characterized by a gradual advancement of the liquid region, followed by a final homogenization stage as the PCM approaches complete melting.

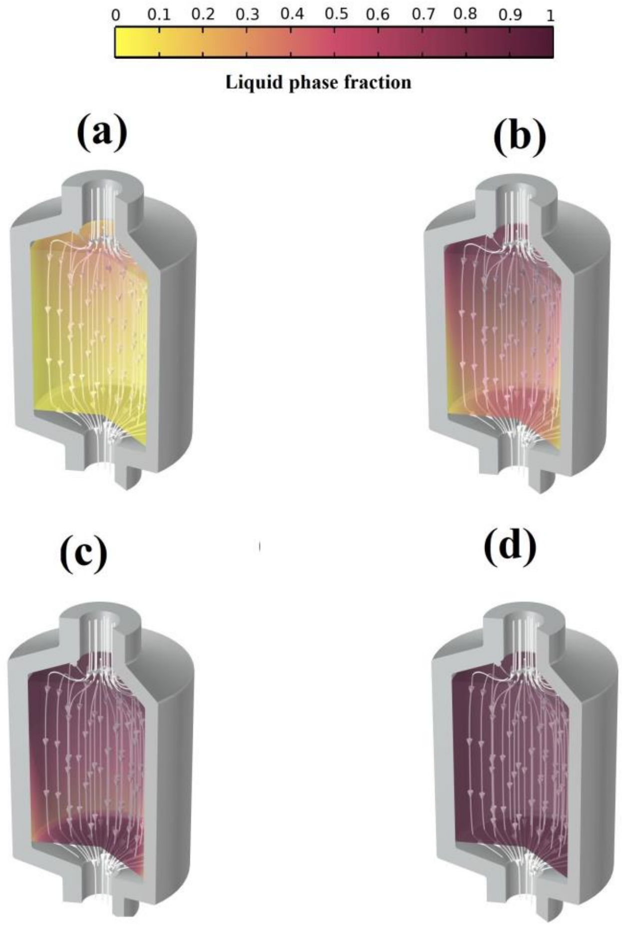

Fig. 8. Phase-field contours during the charging process at (a) 300 min, (b) 420 min, (c) 540 min, and (d) 900 min.

4. Conclusion

A transient numerical model was developed to examine the charging performance of a vertical packed-bed latent heat thermal energy storage unit containing spherical paraffin PCM capsules. The packed capsule region was modeled as an equivalent porous medium, while the heat-transfer fluid and PCM were treated using a local thermal nonequilibrium approach. The model was designed to predict the HTF temperature, PCM temperature, liquid-fraction evolution, pressure loss, and charging time during the charging process.

The numerical model was validated against the experimental data of Nallusamy et al. and showed good agreement with the measured PCM temperature trend. The simulation reproduced the main thermal stages of the packed-bed LHTES unit: initial sensible heating, latent-heat-dominated melting, and final sensible heating after melting.

The comparison of PCM, water, and volume-averaged porous-medium temperatures showed clear local thermal nonequilibrium. At around 200 min, the three temperatures were close to 54–55°C. The PCM reached the melting region near 60°Cat approximately 250 min and remained almost constant until about 490 min. During this interval, the water temperature continued to increase and exceeded 64°C, confirming that the fluid and PCM cannot be accurately represented by a single-temperature model.

After approximately 495–500 min, the PCM temperature increased sharply, indicating the transition from latent heat absorption to sensible heating of the melted PCM. Toward the end of the plotted period, the PCM, water, and averaged porous-medium temperatures approached approximately 66–68°C, showing that thermal nonequilibrium decreases after most of the PCM has melted.

The temperature and streamline contours showed that the flow field becomes established early, while the thermal field evolves gradually. At 15 min, the temperature range was approximately 21.8−25.1°C, indicating weak initial heat penetration. At later times of 270, 420, and 900 min, the contours revealed progressive thermal development and persistent spatial nonuniformity near the wall and flow-transition regions.

The phase-field results demonstrated the melting progression more directly. At 300 min, only part of the PCM had melted, and the phase indicator still varied clearly from region to region. By 420 min, the melted region expanded noticeably. At 540 min, most of the storage region had reached high liquid-fraction values, while only limited delayed regions remaining. At 900 min, the phase-field distribution was nearly uniform and close to 1, indicating near-complete melting of the PCM.

The inlet-flow-rate study for 1.5, 2.5, 3.5, and 4.5 L/min showed that flow rate strongly affects the transient PCM temperature response. The curves approached the melting range near 60°C, but the post-melting temperature rise occurred at different times for each flow rate. The results indicate that increasing flow rate does not always produce the best charging response under a fixed heat-input condition, since higher flow rates reduce both the fluid residence time and the temperature rise per pass.

All in all, the results demonstrate that the charging performance of the packed-bed PCM unit is governed by the combined effects of fluid residence time, interphase heat transfer, latent heat absorption, and spatial flow distribution. The inclusion of quantitative temperature histories, phase-field evolution, and flow-rate comparison provides a clearer basis for evaluating the charging behavior of encapsulated paraffin packed-bed thermal storage systems.

Acknowledgments

The research council at Kermanshah University of Technology (KUT) is highly acknowledged for its support during the course of this project.

Declaration of competing interest

The authors declare no conflict of interest.

Data availability

Data will be made available on reasonable request.

References

[1] T. J. C. Santos, J. M. Torres Farinha, M. Mendes, and J. Monteiro, Thermal Energy Storage in Renewable Energy Communities: A State-of-the-Art Review, Energies, vol. 19, no. 5, p. 1363, 2026. https://doi.org/10.3390/en19051363

[2] A. T. Tafere, Thermal Energy Storage Technologies: A Review of Current Landscape and Future Directions, F1000Research, vol. 15, p. 83, 2026. https://doi.org/10.12688/f1000research.176639.2

[3] F. Han, S. Yu, and S. Sun, The demand-side management control strategy and system optimization of a PV/T-ASHP system with thermal energy storage, Journal of Building Engineering, vol. 117, p. 114908, 2026. https://doi.org/10.1016/j.jobe.2025.114908

[4] D. S. Karpenko, T. O. Yevtukhova, and O. V. Novoseltsev, Energy service business models: Organizational frameworks and market integration enabled by thermal energy storage, Energy Technologies & Resource Saving, vol. 86, no. 1, pp. 42-62, 2026. https://doi.org/10.33070/etars.1.2026.04

[5] L. Romagnoli, Thermal energy storage integration in power system for power-to-heat services, Ph.D. dissertation, Sapienza University of Rome, Rome, Italy, 2026.

[6] P. Jóźwiak, Ł. Topolnicki, H. Sądej, Ł. Szabłowski, and K. Badyda, Assessing the potential of thermal energy storage as a method for achieving increased utilization time of a nuclear power plant in volatile demand for energy in the electrical grid, Energy Conversion and Management, vol. 359, p. 121552, 2026. https://doi.org/10.1016/j.enconman.2026.121552

[7] H. Chater, M. Asbik, L. El-Kaddadi, A. Louanate, and K. El Alami, Exergy analysis and novel topological optimization of fin structures in latent heat thermal energy storage system: Experimental study, Journal of Energy Storage, vol. 121, p. 116478, 2025. https://doi.org/10.1016/j.est.2025.116478

[8] T. B. Erol et al., Expanded graphite enhanced cellulose aerogel/palmityl alcohol composite phase change material with effective thermal energy storage properties, Journal of Energy Storage, vol. 132, p. 117892, 2025. https://doi.org/10.1016/j.est.2025.117892

[9] A. Nandi, N. Biswas, A. Datta, N. K. Manna, D. K. Mandal, and S. Biswas, A comprehensive review on enhanced phase change materials (PCMs) for high-performance thermal energy storage: Progress, challenges, and future perspectives, Journal of Thermal Analysis and Calorimetry, vol. 150, no. 12, pp. 8933-8976, 2025. https://doi.org/10.1007/s10973-025-14301-w

[10] W. K. Jabbar, A. K. Alshara, and A. S. Allawy, Experimental study of solar thermal energy storage finned tanks filled with different storage materials (PCM, gravel, and water), Results in Engineering, vol. 26, p. 105041, 2025. https://doi.org/10.1016/j.rineng.2025.105041

[11] H. Jouhara, A. Żabnieńska-Góra, N. Khordehgah, D. Ahmad, and T. Lipinski, Latent thermal energy storage technologies and applications: A review, Int. J. Thermofluids, vols. 5-6, p. 100039, 2020. https://doi.org/10.1016/j.ijft.2020.100039

[12] A. Sharma, V. V. Tyagi, C. R. Chen, and D. Buddhi, Review on thermal energy storage with phase change materials and applications, Renew. Sust. Energ. Rev., vol. 13, no. 2, pp. 318-345, 2009. https://doi.org/10.1016/j.rser.2007.10.005

[13] S. Pourhemmati, S. Hossainpour, and S. Z. Haeri, Experimental and numerical investigation of packed-bed thermal energy storage utilizing two phase change materials (PCM) in spherical capsules, International Journal of Thermal Sciences, vol. 210, p. 109605, 2025. https://doi.org/10.1016/j.ijthermalsci.2024.109605

[14] T. V. Rocha, Performance characterization of thermal storage tank with phase change material, M.Sc. thesis, Faculty of Engineering, University of Porto, Porto, Portugal, 2025.

[15] P. Mollo, A. Jahanbin, and U. Berardi, Development and validation of a numerical model for packed bed PCM thermal energy storage systems, in International Conference on Construction, Energy, Environment and Sustainability, 2025: Springer Nature, pp. 395-403. https://doi.org/10.1007/978-981-95-1826-5_42

[16] J. N. Omlang and A. Calderon, A review of mathematical reduced-order modeling of PCM-based latent heat storage systems, Energies, vol. 19, no. 9, p. 2017, 2026. https://doi.org/10.3390/en19092017

[17] L. Crnjac, K. Siddiqui, and A. G. Straatman, Heat transfer enhancement to promote melting and solidification in a PCM-based thermal storage module, Journal of Energy Storage, vol. 132, p. 117904, 2025. https://doi.org/10.1016/j.est.2025.117904

[18] J. Li et al., Analysis of heat transfer and fluid flow during the melting process of PCM within tubular thermal energy storage unit, Applied Thermal Engineering, vol. 244, p. 122681, 2024. https://doi.org/10.1016/j.applthermaleng.2024.122681

[19] V. Pabst, Thermal Energy Storage with Zonal Fixed Beds of Phase Change Material: A Simulative and Experimental Investigation, Ulm University, Ulm, Germany, 2024. https://doi.org/10.18725/OPARU-55900

[20] M. A. Lily, T. A. Refat, T. Abedien, A. K. M. Monjur Morshed, and T. C. Paul, Performance analysis of a packed bed latent heat thermal energy storage with encapsulated silica as PCM: Numerical investigation, in Proc. 8th Thermal and Fluids Engineering Conference (TFEC), 2023, pp. 885-888. https://doi.org/10.1615/TFEC2023.esy.046392

[21] T. Saitoh and K. Hirose, High-performance phase-change thermal energy storage using spherical capsules, Chemical Engineering Communications, vol. 41, nos. 1-6, pp. 39-58, 1986. https://doi.org/10.1080/00986448608911711

[22] D. E. Beasley, C. Ramanarayanan, and H. Torab, Thermal response of a packed bed of spheres containing a phase-change material, Int. J. Energy Res., vol. 13, no. 3, pp. 253-265, 1989. https://doi.org/10.1002/er.4440130302

[23] A. F. Regin, S. C. Solanki, and J. S. Saini, An analysis of a packed bed latent heat thermal energy storage system using PCM capsules: Numerical investigation, Ren. Energy, vol. 34, no. 7, pp. 1765-1773, 2009. https://doi.org/10.1016/j.renene.2008.12.012

[24] M. Grabo, E. Acar, and E. Y. Kenig, Modeling and improvement of a packed bed latent heat storage filled with non-spherical encapsulated PCM-elements, Renew. Energy, vol. 173, pp. 1087-1097, 2021. https://doi.org/10.1016/j.renene.2021.04.022

[25] A. de Gracia and L. F. Cabeza, Numerical simulation of a PCM packed bed system: A review, Renew. Sust. Energ. Rev., vol. 69, pp. 1055-1063, 2017. https://doi.org/10.1016/j.rser.2016.09.092

[26] P. Anand, P. K. S. Tejes, B. K. Naik, and H. Niyas, Design analysis and performance prediction of packed bed latent heat storage system employing machine learning models, Journal of Energy Storage, vol. 72, p. 108690, 2023. https://doi.org/10.1016/j.est.2023.108690

[27] M. Zamengo, S. Wu, R. Yoshida, and J. Morikawa, Multi-objective optimization for assisting the design of fixed-type packed bed reactors for chemical heat storage, Applied Thermal Engineering, vol. 218, p. 119327, 2023. https://doi.org/10.1016/j.applthermaleng.2022.119327

[28] S. Trevisan and R. Guédez, Design optimization of an innovative layered radial-flow high-temperature packed bed thermal energy storage, Journal of Energy Storage, vol. 83, p. 110767, 2024. https://doi.org/10.1016/j.est.2024.110767

[29] Q. Mao and W. Cao, Effect of variable capsule size on energy storage performances in a high-temperature three-layered packed bed system, Energy, vol. 273, p. 127166, 2023. https://doi.org/10.1016/j.energy.2023.127166

[30] T. R. Kopparthi, V. Athawale, P. Rath, and A. Bhattacharya, Effect of capsule shape on melting and energy storage rates for encapsulated PCM-based systems, in Proceedings of the 1st International Conference on Fluid, Thermal and Energy Systems: ICFTES 2022, 2024: Springer Nature, pp. 279-290. https://doi.org/10.1007/978-981-99-5990-7_25

[31] P. Lv, L. Liu, G. Lei, and H. Dong, Pore-scale numerical investigation on the thermal storage properties of packed-bed systems with phase change material microcapsules, Journal of Cleaner Production, vol. 405, p. 137071, 2023. https://doi.org/10.1016/j.jclepro.2023.137071

[32] E. S. Reddy, R. M. Reddy, and K. H. Reddy, Experimental and numerical investigation of three phase change materials (PCM) in spherical capsules, Journal of Mechanical Science and Technology, vol. 39, no. 9, pp. 5551-5560, 2025. https://doi.org/10.1007/s12206-025-0854-5

[33] B. Sun, M. Sun, L. Gao, D. Che, and Y. Deng, Thermal performance analysis and optimization of a double-layer spherical phase-change material capsule with annular fins, Journal of Energy Storage, vol. 57, p. 106280, 2023. https://doi.org/10.1016/j.est.2022.106280

[34] J. Yu, Z. Zhang, G. Zhang, X. Liu, and Z. Rao, Investigation of structural influence on the thermal energy storage efficiency in phase change capsules, Thermal Science and Engineering Progress, vol. 67, p. 104122, 2025. https://doi.org/10.1016/j.tsep.2025.104122

[35] R. Ma, Z. Ren, J. Guo, and Y. Wu, Numerical investigation of heat transfer and flow behavior in a 3D void phase change capsule model with nanoparticle-enhanced modified solar salt, Applied Thermal Engineering, vol. 281, p. 128647, 2025. https://doi.org/10.1016/j.applthermaleng.2025.128647

[36] N. Nallusamy, S. Sampath, and R. Velraj, Study on performance of a packed bed latent heat thermal energy storage unit integrated with solar water heating system, J. Zhejiang Univ. Sci. A, vol. 7, no. 8, pp. 1422-1430, 2006. https://doi.org/10.1631/jzus.2006.a1422